



OPEN ACCESS

EDITED BY
Octavian-Dumitru Pavel,
University of Bucharest, Romania

REVIEWED BY
Laura Cocheci,
Politehnica University of Timișoara,
Romania
Haixin Guo,
Tohoku University, Japan

*CORRESPONDENCE
Bálsamo Nancy,
nbalsamo@frc.utn.edu.ar

SPECIALTY SECTION
This article was submitted to Catalytic
Engineering,
a section of the journal
Frontiers in Chemical Engineering

RECEIVED 24 August 2022
ACCEPTED 28 September 2022
PUBLISHED 14 October 2022

CITATION
Dalma A, Nancy B, Griselda E and
Mónica C (2022), Mixed oxides from
calcined layered double hydroxides for
glycerol carbonate production to
contribute to the biodiesel economy.
Front. Chem. Eng. 4:1027152.
doi: 10.3389/fceng.2022.1027152

COPYRIGHT
© 2022 Dalma, Nancy, Griselda and
Mónica. This is an open-access article
distributed under the terms of the
[Creative Commons Attribution License
\(CC BY\)](https://creativecommons.org/licenses/by/4.0/). The use, distribution or
reproduction in other forums is
permitted, provided the original
author(s) and the copyright owner(s) are
credited and that the original
publication in this journal is cited, in
accordance with accepted academic
practice. No use, distribution or
reproduction is permitted which does
not comply with these terms.

Mixed oxides from calcined layered double hydroxides for glycerol carbonate production to contribute to the biodiesel economy

Argüello Dalma, Bálsamo Nancy*, Eimer Griselda and Crivello Mónica

Centro de Investigación y Tecnología Química, CONICET Universidad Tecnológica Nacional, Facultad Regional Córdoba, Córdoba, Argentina

The glycerol generated as a by-product in the production of biodiesel could be used as a renewable raw material to economically promote the production process. The catalytic conversion of glycerol to a product with higher added value, such as glycerol carbonate, has attracted great interest in the chemical, pharmaceutical, and lithium battery industries, among others, due to its low toxicity, hydration capacity, and biodegradability. Layered-double hydroxide (LDH) materials, the precursors of the catalysts, were synthesized by a direct coprecipitation method to incorporate a third metal ion in addition to magnesium and aluminum ions. This method is the easiest regularly applied technique to design these low cost anionic nanoclay. The atomic percentage of Cu, Zn, or Ni incorporated was 15% of the Mg load in the material. The synthesis atomic ratio, $(M^{2+} + Mg^{2+})/Al^{3+}$ had a constant value of 3, where M represents the transition metal incorporated. LDHs produced the corresponding mixed metal oxides by thermal decomposition. These materials have excellent properties for reactions catalyzed by the basic sites, high surface area, homogeneous cation dispersion, and thermal stability. The physicochemical material properties were characterized by XRD, N_2 sorption, MP-AES, TPD- CO_2 , SEM, and XPS. The mixed oxides were evaluated in the catalytic conversion of glycerol to glycerol carbonate. The addition of Cu, Ni, or Zn to the matrix of Mg and Al produced changes in its physicochemical properties and mostly in the catalytic activity. X-ray diffractograms of LDHs showed the typical characteristic structure of layers even with metallic ions of Cu, Ni, or Zn incorporated, because their ionic radii are similar to that of the Mg ion, 0.69, 0.73, and 0.74 Å, respectively. The obtained mixed oxides showed a high catalytic activity towards the conversion of glycerol to glycerol carbonate under mild reaction conditions, a 1:2 ratio of glycerol:ethylene carbonate and solvent free. Relative yields higher than 80% were obtained, attributable to an adequate distribution of basicity and textural parameters. The catalysts were used in successive reaction cycles without significant loss of activity.

KEYWORDS

layered double hydroxides, mixed oxides, heterogeneous catalysis, glycerol, glycerol carbonate

Introduction

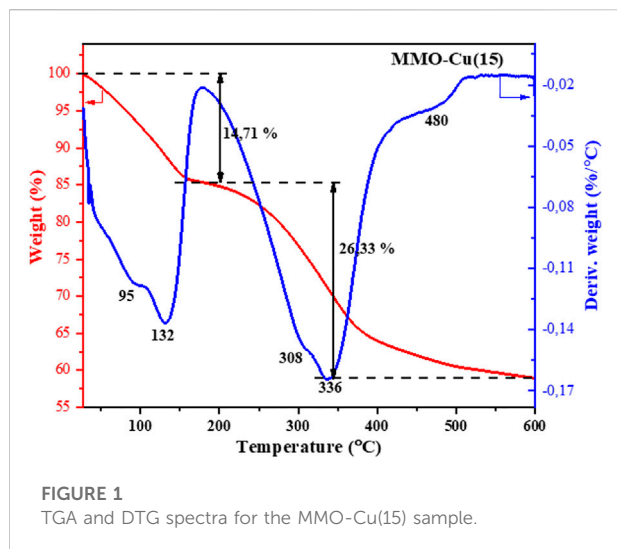
The circular economy provides a new way to produce and consume. The possibilities for economic development associated with the circular economy always promote sustainable development (Jaiswal et al., 2022). Here, biodiesel is among the most commonly used renewable energy sources. Biodiesel production generates 10% by weight of glycerol as a by-product, so it is reasonable to consider its employment as a renewable raw material to economically advantage the process. The catalytic conversion of glycerol (Gly) to a product with high value, such as glycerol carbonate (GC), has attracted great interest due to its low toxicity, hydration capacity, and biodegradability (Sonnati et al., 2013; Lukato et al., 2021). The transesterification reaction demands glycerol and the availability of another precursor molecule, such as an alkyl carbonate (Esteban et al., 2015a; Esteban et al., 2015b; Kondawar and Rode, 2017; Pradhan and Sharma, 2020). Alkyl carbonates, such as ethylene carbonate (EC), a cyclic organic carbonate, produce ethylene glycol, a valuable by-product, together with the glycerol carbonate (Esteban et al., 2016). The GC is a building block for polycarbonates, a green solvent, and an additive in the electrolytic solutions used in lithium batteries, cosmetics, food, and the medical industry (Sonnati et al., 2013; Christy et al., 2018). For the synthesis of glycerol carbonate, many catalysts, such as zeolites (Singh et al., 2014), metal salts (Procopio and Di Gioia, 2022), zinc catalysts (Fujita et al., 2013), ionic liquids immobilized on resins (Cho et al., 2010; Kim et al., 2011), metal oxides (Deshmukh and Yadav, 2021), and hydrotalcites (Climent et al., 2010; Galadima and Muraza, 2017) have been studied. In all such studies, a strong relationship is evidenced between the catalytic activity and the balance of basic sites, which show a higher yield of glycerol carbonate. Among the catalysts reported, layered double hydroxides (LDHs) as precursors of mixed metal oxides stand out as heterogeneous catalysts, producing high yields and leaching resistance compared to other solid catalysts (Lari et al., 2017). As a sustainable alternative means of producing GC, transesterification between glycerol and an alkyl carbonate has been proposed, using mixed metal oxides (MMO) derived from LDH (Climent et al., 2010). LDHs are anionic nanoclays with a lamellar structure. The general formula is $[M^{2+}_{(1-x)}M^{3+}_x(OH)_2]^{x+}(A^{n-})_{x/n} \cdot mH_2O$, where M^{2+} and M^{3+} refer to mono, di, tri, and tetravalent metal ion placed in the layers as hydroxides, while A represents the charge compensating anion, generally carbonate, which, together with m water molecules, are located in the inter lamellar space; x can vary between 0.17 and 0.33, depending on the combination of di and trivalent metals. Meanwhile, when only Mg and Al metal cations are present in the nanoclay composition, the material is called

hydrotalcite (HT). The properties of LDH are strongly influenced by the composition and nature of the anions and cations of the structure. The incorporation of a third metal in the structure modifies its catalytic behavior. The LDH also exhibits catalytic behavior to synthesize glycerol carbonate, as previously noted, only the MMO obtained were tested in this work. Thus, the MMO were evaluated directly to determine best glycerol carbonate yield (Granados-Reyes et al., 2016). On the other hand, the MMOs derived from LDH form a homogeneous composition at the molecular scale and show behavior that is distinct from the behavior of pure metal oxides. Due to the combination of different phases in the molecular network, they present high surface area, thermal stability, basic surface properties, and homogeneous dispersion of the active phase (Corma et al., 2005; Crivello et al., 2005). In this work, the catalytic results of glycerol conversion to glycerol carbonate through MMOs with the incorporation of different transition metals (Cu, Ni, or Zn) are presented, focusing on the selectivity to glycerol carbonate, maximized over the glycidol produced and the stability of materials during recycling.

Materials and methods

Catalysts synthesis

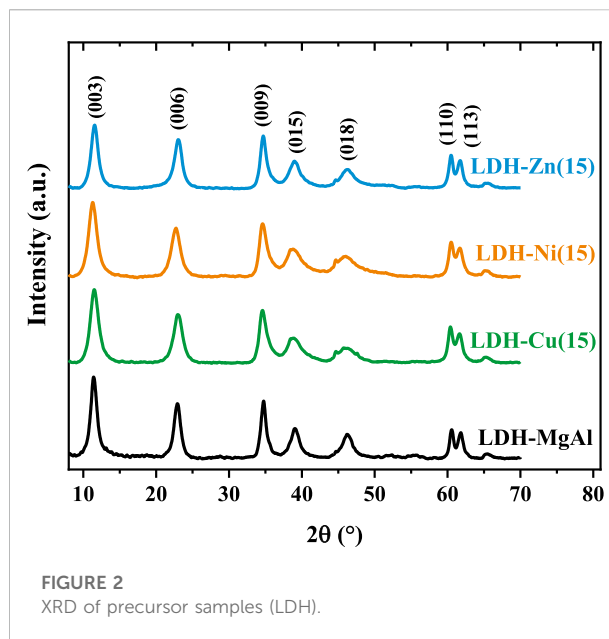
The precursors, LDH materials, were synthesized by the direct coprecipitation method to incorporate the metal ions. The atomic percentages of Cu, Zn, or Ni incorporated were 15%, replacing the Mg load in the material (Bálsamo et al., 2017; Bálsamo et al., 2020; Rizescu et al., 2020). The 15% level was chosen for the second divalent metal in the structure after the 15%, 20%, and 25% levels were evaluated. The MMO with 15% for the second divalent metal incorporated presented the best performance. The detailed results are not shown in this work. The selection was also based on the range adopted by Marimuthu et al. (2018) (from 13% to 27%) on the best catalytic behavior. The atomic ratio of the synthesis, $(M^{2+}+Mg^{2+})/Al^{3+}$, showed a constant value of 3 (where M indicates the transition metal incorporated). The method consisted of the dropwise addition of two prepared solutions, one of them from the nitrates of Mg and Al and of the transition metal to be incorporated. The other one was a Na_2CO_3 solution that provides the interlayer anion to be achieved the structure. In addition, a NaOH solution was added to keep the pH constant at 10 ± 0.2 and to promote the hydroxide formation. The gel obtained was stirred continuously for 4 h, and an aging period of 18 h was followed. The precipitate obtained was filtered and washed with distilled water up to pH 7. After washing, the sample was dried in an oven at 90°C for 12 h



(Bálsamo et al., 2020). The precursors were calcined at 450°C for 9 h to obtain the MMO. The option of the calcination temperature (450°C) for obtaining the mixed metal oxides was defined through the thermal decomposition of the hydroxalcalite-like compounds into mixed oxides was studied. Water at the surface and in the interlayer was eliminated at 105°C and 205°C, respectively. After 370°C the thermogravimetric analysis showed that most interlayer negative ions were eliminated. A slight maximum at about 480°C was presented in the DTG analysis attributed to residual nitrates ion remaining after washing of the LDH sample, which agrees with the reported results (Basag et al., 2016). Consequently, the selected calcination temperature of 450°C for obtaining the mixed metal oxides was enough for the oxide phase appearance, as shown by TGA (Kuljiraseth et al., 2019). The TGA and DTG spectra for the MMO-Cu(15) sample are shown in Figure 1 as an example of the thermal behavior of the material. The samples were designated as follows: LDH-M(15) and MMO-M(15), where M indicates the transition metal incorporated.

Catalyst characterization

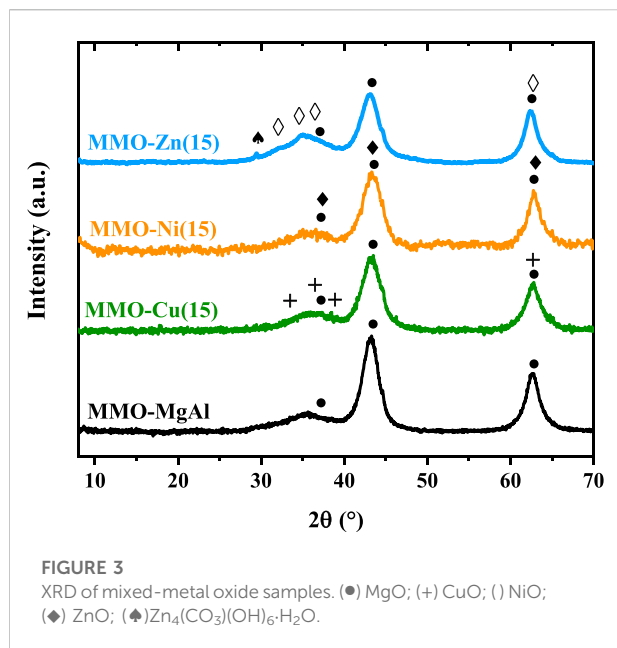
To study the crystalline structure and the different phases present, the materials were characterized by X-ray diffraction (XRD) using an X'Pert Pro-PANalytical diffractometer equipped with CuK α radiation ($\lambda = 1.54 \text{ \AA}$). Diffraction patterns were collected in a 2θ range from 4° to 70° with a step of 0.03 and 4.5 s/step. Elemental analysis was carried out by microwave plasma atomic emission spectrometry (MP-AES) in an Agilent 4200 equipment (Agilent, United States) after dissolving the samples with acid digestion, according to the US EPA 3052A method. The surface area and pore characteristics of the calcined materials were determined by



N₂ sorption analysis at -196°C using an ASAP 2020 Plus 2.0 equipment (Micromeritics, United States). The Brunauer-Emmett-Teller (BET) equation was applied to calculate the surface area. Measurements of pore size and pore volume were obtained from desorption isotherm analysis using the Barrett-Joyner-Halenda (BJH) method. The catalyst morphology was observed by high-resolution scanning electron microscopy (SEM) in a Sigma-ZEISS equipment. By desorption at programmed temperature with a CO₂ probe molecule (TPD), the basicity of the MMO surface was determined using a Chemisorb 2720 (Micromeritics, United States). The X-ray photoelectron spectroscopy (XPS) measurements were performed using a Thermo Scientific K-Alpha spectrometer, equipped with a reduced spot aluminum (Al K $\alpha = 1486.6 \text{ eV}$) monochromatic X-ray source and a hemispherical analyzer with 180° double focus and 128-channel detector. Charge effects were compensated for by using an electron gun. Peak fitting involved a Shirley-type baseline subtraction and subsequent deconvolution using mixed Gaussian-Lorentzian functions. This analysis was performed using Avantage software. Binding energy (BE) values were referenced to C 1 s at 284.8 eV.

Catalytic reactions

The reactions were performed in a glass batch reactor (20 ml) equipped with a condenser system. The reactor was operated in a batch regime with the solid and liquid phases stirred at atmospheric pressure. The reaction parameters were modified until those that determined the maximum yield for glycerol



carbonate from the reaction between glycerol (Cicarelli, 99%) and ethylene carbonate (Aldrich, 98%) were achieved; a molar ratio Gly:EC of 1:2 was used. The reactions were carried out at 70°C during 90 min, solvent free, using 7.5% catalyst by weight from glycerol weight. After the reaction time, the solid catalyst was separated by centrifugation and the liquid reaction mixture was analyzed by gas chromatography. Stability material studies also incorporated in the separation of the used catalyst from the reaction mixture by centrifugation and acetone washing, followed by drying at 100°C overnight. An Agilent Technologies 7820A gas chromatography device with an HP-20M capillary column (25 m × 0.20 mm × 0.20 μm) and a flame ionization detector was employed. The identification and quantification were carried out using the standards of 4-(Hydroxymethyl)-1,3-dioxolan-2-one (Sigma Aldrich, >99% GC) and Glycidol (Sigma Aldrich, >99% GC). A known amount of cyclohexanol (Sigma Aldrich, >99% GC) was added as an internal standard to quantifies conversion, yield, and selectivity results.

Results and discussion

The LDH diffractograms are shown in Figure 2. Typical diffraction peaks at $2\theta \sim 11^\circ$, 22° , and 35° corresponding to the (003), (006), and (012) crystal planes in the layered structures with a rhombohedral symmetry (3R) were observed in all samples (Fu et al., 2021). The thermal decomposition treatment of the LDH at 450°C destroyed the lamellar structure, and it also allowed the formation of metal oxides. The MMO diffractograms (Figure 3) exhibited peaks at 2θ of 37° ,

43° , and 63° and were assigned to reflections of the periclase phase of MgO (JCPDS 00-001-1235) (Sangeetha et al., 2019). No segregated phases were detected, which suggests that the transition metal oxides were homogeneously dispersed in the matrix of Mg and Al oxides. Thereby, the slight and widened diffraction peaks correspond to the CuO, NiO, or ZnO phases in MMO-Cu(15), MMO-Ni(15), and MMO-Zn(15), respectively. Specifically, in the MMO-Cu(15) sample, diffraction peaks at $2\theta = 32^\circ$, 36° , 39° , and 62° are characteristic of CuO (JCPDS 00-002-1041). The signals at $2\theta = 37^\circ$, 43° , and 63° in the MMO-Ni(15) sample can be attributed to NiO (JCPDS 00-001-1239). Finally, the peaks at $2\theta = 32^\circ$, 34° , 36° , and 63° for the diffractogram of the MMO-Zn(15) sample correspond to the ZnO phase (JCPDS 00-001-1136); the slight peak at $2\theta = 29^\circ$ can be attributed to the remaining intermediate phase of zinc carbonate (Sangeetha et al., 2019).

Table 1 shows the cell parameters for the hydroxalcalite-type compounds. Assuming hexagonal symmetry, these parameters are calculated through the reflections (003) and (110), using the equations $c = 3d_{003}$ and $a = 2d_{110}$, where c indicates the basal spacing (between layers), and a is the average cation-cation distance in the lamellar structure (Luggren et al., 2016). It was observed that the cation-cation distance and the basal spacing were similar in the precursors substituted with the transition metal and in the HT. The average crystallite size of the precursors in the “c” direction (the stacking direction, which is perpendicular to the layers) was estimated from the (003) reflection using the Debye-Scherrer equation (Xu and Zeng, 2000). Although the mean size of the crystallites in the “a” direction was estimated from the FWHM of the (110) peak (Zhang et al., 2004), the low intensity of this peak together with the approximations inherent in the Scherrer equation introduces significant uncertainty to the calculated value (de Souza Rossi et al., 2019). The values of the crystallite size of the precursors oscillated between 6.5 and 8.7 nm for the LDH with the Cu or Zn incorporated and the MgAl sample, respectively, and they were similar to those previously reported (Di Cosimo et al., 1998; Kannan et al., 2005; Valente et al., 2010; Başağ et al., 2016) (Table 1). The precursors with the transition metal presented smaller crystallite sizes than the HT. The crystallite sizes of the mixed oxides (Table 2) were estimated by applying the Debye-Scherrer equation to (200) reflection and using the inter-planar distance of the cubic cell ($d_{hkl} = a/\sqrt{h^2 + k^2 + l^2}$). The morphology values identified were close, ranging from 3.3 nm for the MMO with Ni incorporated to 4.0 nm for MMO of MgAl. In particular, the size of the crystallites in the MMO, after heat treatment, was lower than the precursor size. Small MgO crystallite sizes favor the dispersion of the active phase in the mixed oxide (Liu et al., 2013). The slight increase in the crystalline particle size of the reused catalysts with the best performance could be attributed to the aggregated phases.

The chemical composition of the samples in the bulk and the surface of the materials is summarized in Table 2 in the MP-AES

TABLE 1 Cell parameters and morphology of the materials.

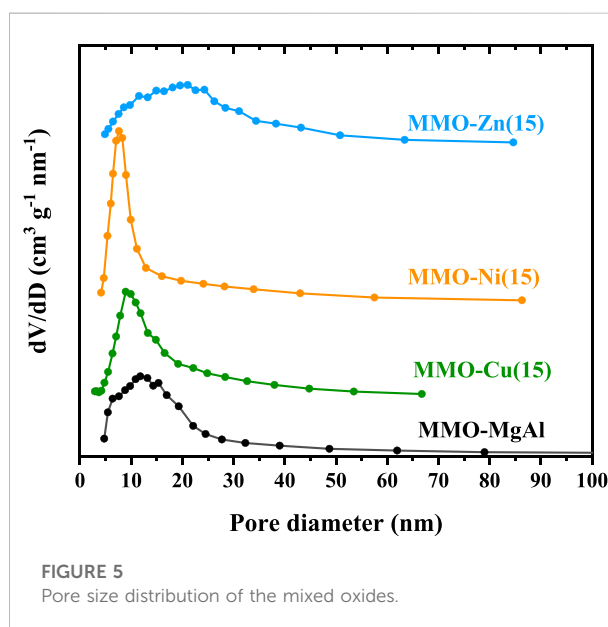
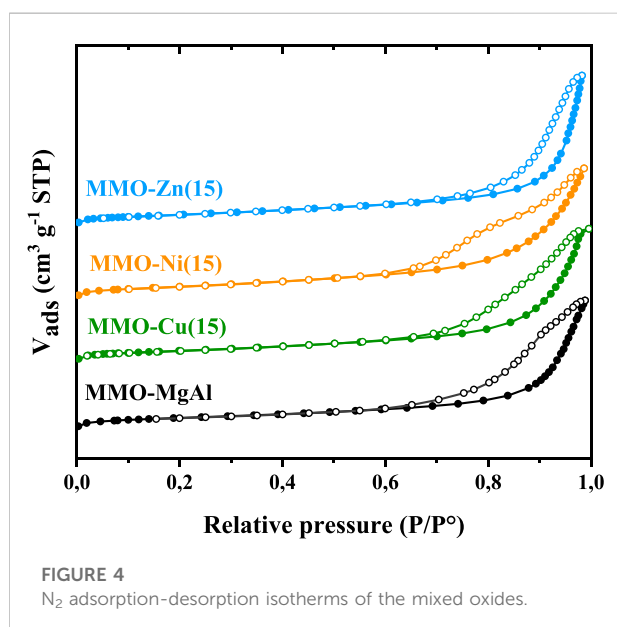
Sample	LDH			MMO				
	Cell parameters			Crystallite size (nm)	Cell parameter (nm)		Crystallite size (nm)	
	d003 (nm)	a (nm)	c (nm)		Fresh	Used*		
MgAl	0.772	0.3052	2.312	8.7	0.4193	4.0	--	
Cu(15)	0.768	0.3065	2.302	6.5	0.4187	3.4	--	
Ni(15)	0.784	0.3057	2.348	6.5	0.4178	3.3	3.5	
Zn(15)	0.761	0.3054	2.279	7.7	0.4199	3.5	3.8	

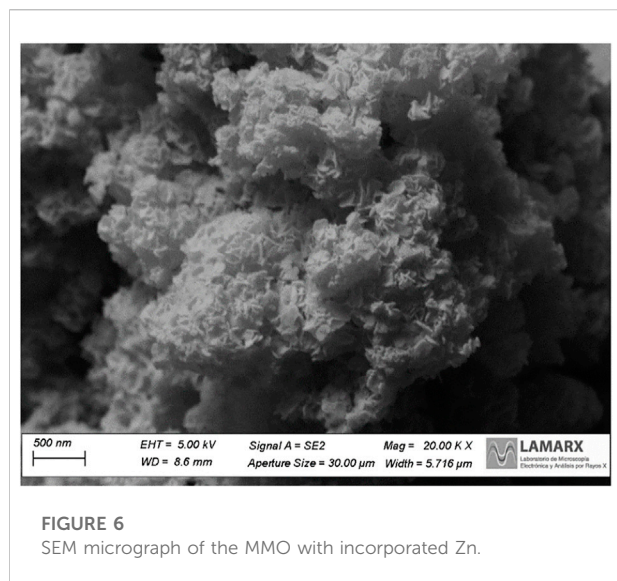
*Corresponding to the catalyst used during four cycles at the reaction conditions: 70°C, 90 min, 7.5% w/w catalyst and reagents molar ratio (Gly:EC) of 1:2.

TABLE 2 Textural properties and metallic composition of the materials.

Sample	LDH	MMO	MMO	M (at%)		(M + Mg)/Al (at%)		Al _s /Al _b *	
	Area (m ² g ⁻¹)	Pore diameter (nm)	Pore volume (cm ³ g ⁻¹)	MP-AES	XPS	MP-AES	XPS		
				MgAl	110	253	14.00		0.711
Cu(15)	120	248	13.62	0.734	15.25	15.25	3.04	0.90	2.13
Ni(15)	119	247	11.28	0.710	15.45	13.72	3.06	1.33	1.74
Zn(15)	118	241	17.48	0.794	14.23	14.35	2.96	1.08	1.42

*Al_s = surface Al (by XPS), Al_b = bulk Al (by MP-AES).





and XPS studies, respectively. The MP-AES results showed that both the atomic percentage ratios of the metal ions and the loads of the transition metals were similar to the theoretical ones. The results obtained by XPS showed that in all cases, there was an enrichment of Al ion content on the surface of the MMO, as evidenced in the atomic percentage ratio of metal ions (Márquez et al., 2001). The enrichment of Al content on the material surface was illustrated in Table 2 by the relation Als/Alb for all samples, where Als indicates the Al content on the surface and Alb indicates the Al content in the bulk, respectively (Birjega et al., 2005; Shen et al., 2017; Arias et al., 2021).

The textural properties of the materials were determined by N₂ adsorption-desorption (Figure 4), and the results are registered in Table 2. As expected, the MMO samples exhibited a higher specific surface area than their precursors due to loose CO₃²⁻ anions such as CO₂ during the calcination process. The surface area slightly decreased with the incorporation of the transition metal (Sahani et al., 2021). According to the IUPAC classification, all of the MMO samples exhibited type IV isotherms with H3 hysteresis loops indicating the presence of mesopores, a result that is confirmed

by pore size distribution (Marimuthu et al., 2018; Rizescu et al., 2020). The hysteresis loops indicate that slit-like pores are formed by the collapse of the layers during calcination treatment (Figure 5). The sizes of the pores and their volumes were similar in all samples of the MMO (Table 2), although a slight increase in those morphologic properties was observed in the MMO with Zn incorporated. The morphology of all MMOs was similar, so the one with a Zn sample incorporated was taken as representative and is depicted in Figure 6. A typical rosette-like structure was detected in the morphology of the MMO samples. No segregated phases were observed when incorporating the different transition metals in the material, which could indicate the successful dispersion of CuO, NiO, or ZnO particles on the matrix of magnesium and aluminum oxides with a strong surface synergism. These surface morphologies were consistent with the analysis carried out on the adsorption-desorption isotherms of N₂ (Climent et al., 2010).

Temperature-programmed desorption studies with CO₂ probe molecule were performed to analyze the strength and percentage of the basic site type present on the surface of the catalysts (Table 3). This material property could perform a key role in the reaction between glycerol and ethylene carbonate because an adequate strength of the basic sites could allow proton extraction from the primary hydroxyl group of glycerol and improve the nucleophilicity of this molecule (Esteban and Vorholt, 2018; Sahani et al., 2021). The desorption profiles were deconvoluted, and three main areas of 50–300°C, 300–500°C, and 500–950°C were distinguished, associated with weak, medium, and strong basic sites, respectively (Figure 7). The weak basic sites correspond to surface OH⁻ groups; the acid-base pairs of M^{x+}–O²⁻ match the medium basic sites, and the strong basic sites are associated with isolated low-coordination anions of O²⁻ (Shi et al., 2021). In particular, the MMO-Cu(15) sample showed a high-temperature desorption peak (860°C), indicating a further increase in the basicity strength of the sites (Climent et al., 2010). A detail analysis of the strength and percentage of each basic site type showed that MMO with Ni or Zn incorporated presented the greater amount of basic sites suitable for transesterification reaction than the remainder of the catalysts. The catalytic

TABLE 3 Basic properties and catalytic activity of the mixed oxides.

MMO	Number of basic sites (mmole g ⁻¹) and percentage (%)				Catalytic activity (mole %)		
	Weak	Medium	Strong	Total	Gly conversion	CG selectivity	GD selectivity
MgAl	1.0 (44)	0.6 (28)	0.6 (28)	2.2	95.9	89.4	10.6
Cu(15)	0.7 (45)	0.4 (27)	0.4 (28)	1.5	95.6	93.6	6.4
Ni(15)	1.7 (53)	0.4 (11)	1.2 (36)	3.2	91.8	96.9	3.1
Zn(15)	1.2 (40)	0.8 (27)	1.0 (33)	2.9	90.5	95.3	4.7

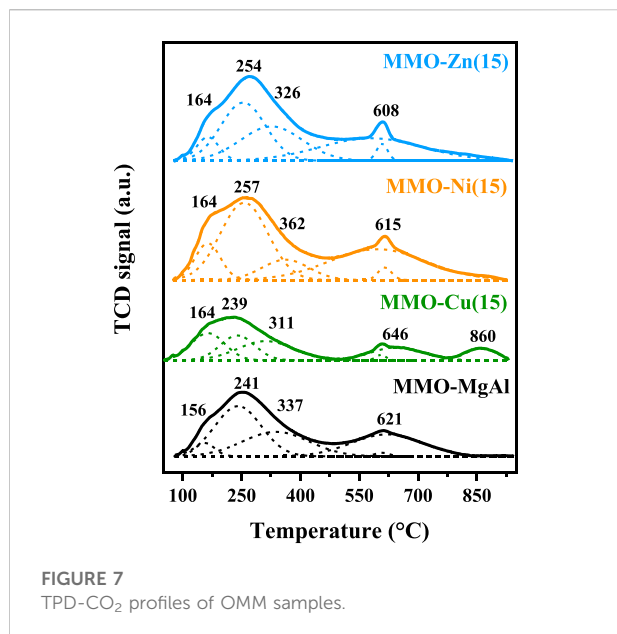


FIGURE 7
TPD-CO₂ profiles of OMM samples.

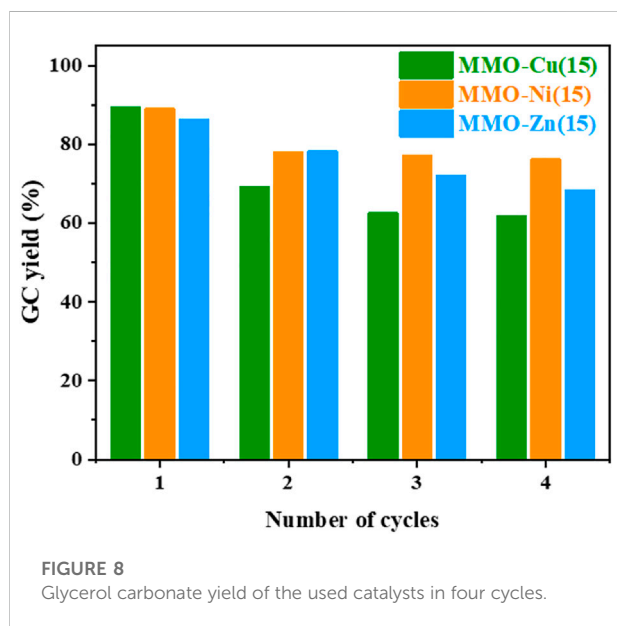


FIGURE 8
Glycerol carbonate yield of the used catalysts in four cycles.

activity of the MMO samples for the transesterification reaction is summarized in Table 3. The transition metal incorporated promoted the glycerol conversion and the selectivity to GC, although a small amount of glycidol (GD) was produced by the decarbonylation of GC as byproduct with the release of CO₂. The reaction parameters mentioned in the methodology were chosen from previous optimization studies. The selectivity and yields obtained are relative to the CG and glycidol (GD) formed (Wang et al., 2018). Table 3 summarizes

TABLE 4 Comparison of the metal composition in the bulk of the synthesis, fresh and used catalysts determined by MP-AES analysis.

MMO	Bulk	M* (% at.)	Mg (% at.)	(M + Mg)/Al
Cu(15)	Theoretical	15,0	85,0	3,0
	Fresh	15,2	84,8	3,0
	Used	15,6	84,4	2,9
Ni(15)	Theoretical	15,0	85,0	3,0
	Fresh	15,5	84,5	3,1
	Used	14,0	86,0	2,9
Zn(15)	Theoretical	15,0	85,0	3,0
	Fresh	14,2	85,8	3,0
	Used	14,7	85,3	2,7

*M = Cu, Zn, or Ni.

the catalytic activity of the MMO catalysts for the transesterification reaction between glycerol and EC at 90 min of reaction. In general, the introduction of the transition metal favored the conversion and selectivity to CG in reference to MMO-MgAl. Even though the GC yields were similar, the MMO-Ni15 catalyst achieved a lower glycidol formation. To obtain information on the stability of the catalysts, the MMOs were reused for four cycles in the transesterification reaction under the same conditions and the results are presented in Figure 8. The catalytic behavior of the MMO-Cu(15) sample showed that the GC yield was sharply reduced throughout the four reuse cycles. The MMO-Zn(15) and MMO-Ni(15) catalysts remained more stable, and the best performance among the four reaction cycles was seen in the latter. This trend can be related to the number of total basic sites (Table 3). In detail, the second cycle for the MMO-Cu(15) sample showed a 20% decrease yield of GC. This catalyst behavior could be attributed to the post reaction treatment, considering that the material was washed with ethanol immediately before each cycle instead of repeat calcination process being applied for activation. The bulk composition of the catalysts is presented in Table 4. The bulk composition of the MMO-Cu(15) sample showed no considerable changes in composition, so this metal leaching should not be attributed. A slight decrease in the Mg atomic % in the used MMO-Cu(15) could be the cause of decreased yield. Considering the basic surface properties, only the sample with Cu incorporated showed less basic strength distribution on the surface, which could potentially have affected the catalytic performance of the mixed oxide. Table 4 shows the bulk metal composition of the fresh and used catalysts. The samples with Cu and Zn incorporated showed a slight

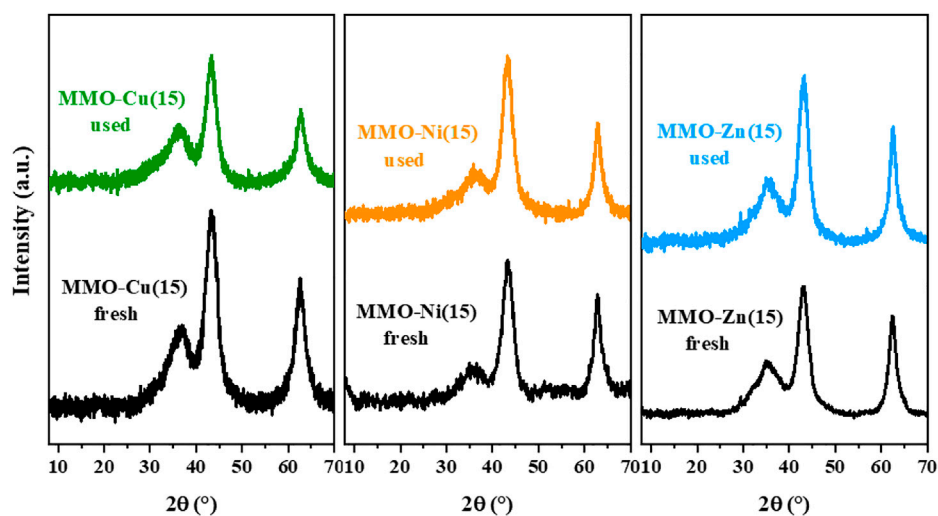


FIGURE 9
XRD of the fresh and used mixed oxides in the transesterification reaction.

decrease in the Mg atomic percentage, while the used sample with Ni incorporated showed a decreased Ni atomic percentage. Although the binary MgAl hydrotalcite with a Mg/Al atomic ratio of 3.0 showed high glycerol conversion under similar reaction conditions, the presence of Cu, Ni, or Zn was essential for the enhancement on the results to occur. The main role of Zn, Ni, or Cu on the catalyst should be attributed to the contribution on the acid-base bifunctional property on the catalyst surface suggested by the role given to the acidic sites. As Kondawar and Rode proposed, the higher catalytic activity of mixed oxides than single metal oxides was promoted by the two activation modes. First, the Lewis basic site of the bifunctional catalyst abstracted a proton from the primary hydroxyl group of glycerol to enhance the nucleophilicity of glycerol. Then, the Lewis acidic site simultaneously activated the carbonyl carbon of alkyl carbonate. Following this, glycerol carbonate was achieved as a product (Kondawar and Rode, 2017). The acid contribution of Cu, Ni, or Zn in the catalytic properties of the materials will be considered in future studies of pyridine FT-IR. The XRD patterns of the fresh and used MMOs after the four cycles, are shown in Figure 9. No phase changes were observed, and the structures were maintained. Consequently, due to the catalytic results of the catalyst reuse and their subsequent physicochemical characterization, the MMO-Ni(15) showed the best performance with great catalytic stability. This could be attributed to a greater number of basic sites than the rest of the catalysts.

Conclusion

The third transition metal ions of Cu, Ni, or Zn were incorporated by coprecipitation in the layered structure of LDHs. No segregated phases of CuO, NiO, or ZnO were detected in the mixed oxides of Mg and Al. These materials presented optimal textural parameters and basic surface properties. All of the mixed metal oxides were catalyst-efficient for the transesterification reaction between glycerol and ethylene carbonate. They could also be reused in four reaction cycles without significant loss of catalytic activity. The MMO-Ni(15) presented the highest stability, followed by MMO-Zn(15) and MMO-Cu(15). This deactivation may be related to a trend in the decrease of the total basic sites for each material. The XRD studies determined that MMO structures were preserved, even after being used. The MMO-Ni(15) showed the best catalytic performance, highest surface number of basic sites, and structural stability.

Data availability statement

The original contributions presented in the study are included in the article/supplementary material, further inquiries can be directed to the corresponding author.

Author contributions

All authors contributed to the article and approved the submitted version.

Funding

The National Technological University has financed the R&D Projects approved and executed in the Chemical Research and Technology Center—CITeQ: 1) Project: MAUTICO0007835TC, “Mixed oxides applied to the sustainable transformation of residual biomass from the olive and biodiesel industries.” Director: Dra. BN. The aforementioned project has received a budget of \$38,000.00 in 2020 and \$50,000.00 in 2021 to finance experimentation and characterization research. Validity period: 2020–2022. 2) Project: IAN4978 “Synthesis and characterization of mixed metal oxides and their evaluation in the recovery of residual biomass of regional interest.” Director: Dra. BN. This project had a budget of \$78,500.00 to finance experimentation and characterization research. Period of validity: 2018–2019.

Acknowledgments

The authors thank the Secretary of Science, Technology and Postgraduate Studies of the National Technological University,

References

- Arias, S., González, J. F., Sousa, L. V., Barbosa, C. B. M., Silva, A. O. S., Fréty, R., et al. (2021). Influence of Ni/Al ratio on the fast pyrolysis of myristic acid when adsorbed on unsupported mixed oxides derived from layered double hydroxides. *Catal. Today* 381, 181–191. doi:10.1016/j.cattod.2020.07.028
- Bálsamo, N. F., Sapag, K., Oliva, M. I., Pecchi, G. A., Eimer, G. A., and Crivello, M. E. (2017). Mixed oxides tuned with alkaline metals to improve glycerolysis for sustainable biodiesel production. *Catal. Today* 279 (2), 209–216. doi:10.1016/j.cattod.2016.06.005
- Bálsamo, N., Mendieta, S., Heredia, A., and Crivello, M. (2020). Nanoclays as dispersing precursors of La and Ce oxide catalysts to produce high-valued derivatives of biodiesel by-product. *Mol. Catal.* 481, 110290. doi:10.1016/j.mcat.2019.01.010
- Basąg, S., Piowowska, Z., Kowalczyk, A., Węgrzyn, A., Baran, R., Gil, B., et al. (2016). Cu-Mg-Al hydrotalcite-like materials as precursors of effective catalysts for selective oxidation of ammonia to dinitrogen — The influence of Mg/Al ratio and calcination temperature. *Appl. Clay Sci.* 129, 122–130. doi:10.1016/j.clay.2016.05.019
- Birjega, R., Pavel, O. D., Costentin, G., Che, M., and Angelescu, E. (2005). Rare-earth elements modified hydrotalcites and corresponding mesoporous mixed oxides as basic solid catalysts. *Appl. Catal. A General* 288 (1–2), 185–193. doi:10.1016/j.apcata.2005.04.030
- Cho, H.-J., Kwon, H.-M., Tharun, J., and Park, D.-W. (2010). Synthesis of glycerol carbonate from ethylene carbonate and glycerol using immobilized ionic liquid catalysts. *J. Ind. Eng. Chem.* 16 (5), 679–683. doi:10.1016/j.jiec.2010.07.019
- Christy, S., Noschke, A., Lomeli-Rodriguez, M., Greeves, N., and Lopez-Sanchez, J. A. (2018). *Green Sustain. Chem* 14, 99–107.
- Climont, J., Corma, A., De Frutos, P., Iborra, S., Noy, M., Veltý, A., et al. (2010). Chemicals from biomass: Synthesis of glycerol carbonate by transesterification and carbonylation with urea with hydrotalcite catalysts. The role of acid–base pairs. *J. Catal.* 269 (1), 140–149. doi:10.1016/j.jcat.2009.11.001
- Corma, A., Hamid, S., Iborra, S., and Veltý, A. (2005). Lewis and Brønsted basic active sites on solid catalysts and their role in the synthesis of monoglycerides. *J. Catal.* 234, 340–347. doi:10.1016/j.jcat.2005.06.023
- Crivello, M., Pérez, C., Herrero, E., Ghione, G., Casuscilli, S., and Rodríguez-Castellón, E. (2005). Characterization of AlCu and AlCuMg mixed oxides and their catalytic activity in dehydrogenation of 2-octanol. *Catal. Today* 107, 215–222. doi:10.1016/j.cattod.2005.07.168
- de Souza Rossi, J., Perrone, O. M., Siqueira, M. R., Volanti, D. P., Gomes, E., da Silva, R., et al. (2019). Effect of lanthanide ion doping on Mg–Al mixed oxides as active acid–base catalysts for fatty acid ethyl ester synthesis. *Renew. Energy* 133, 367–372. doi:10.1016/j.renene.2018.10.038
- Deshmukh, G. P., and Yadav, G. D. (2021). Tuneable transesterification of glycerol with dimethyl carbonate for synthesis of glycerol carbonate and glycidol on MnO₂ nanorods and efficacy of different polymorphs. *Mol. Catal.* 515, 111934. doi:10.1016/j.mcat.2021.111934
- Di Cosimo, J. I., Díez, V. K., Xu, M., Iglesia, E., and Apesteguía, C. R. (1998). Structure and surface and catalytic properties of Mg–Al basic oxides. *J. Catal.* 178, 499–510. doi:10.1006/jcat.1998.2161
- Esteban, J., Dominguez, E., Ladero, M., and García-Ochoa, F. (2015). Kinetics of the production of glycerol carbonate by transesterification of glycerol with dimethyl and ethylene carbonate using potassium methoxide, a highly active catalyst. *Fuel Process. Technol.* 138, 243–251. doi:10.1016/j.fuproc.2015.06.012
- Esteban, J., Fuente, E., Blanco, A., Ladero, M., and García-Ochoa, F. (2015). Phenomenological kinetic model of the synthesis of glycerol carbonate assisted by focused beam reflectance measurements. *Chem. Eng. J.* 260, 434–443. doi:10.1016/j.cej.2014.09.039
- Esteban, J., Ladero, M., Fuente, E., Blanco, A., and García-Ochoa, F. (2016). Experimental and modelling approach to the catalytic coproduction of glycerol carbonate and ethylene glycol as a means to valorise glycerol. *J. Taiwan Inst. Chem. Eng.* 63, 89–100. doi:10.1016/j.jtice.2016.03.031
- Esteban, J., and Vorholt, A. J. (2018). Obtaining glycerol carbonate and glycols using thermomorphic systems based on glycerol and cyclic organic carbonates: Kinetic studies. *J. Ind. Eng. Chem.* 63, 124–132. doi:10.1016/j.jiec.2018.02.008
- Fu, X., Ren, X., Shen, J., Jiang, Y., Wang, Y., Orooji, Y., et al. (2021). Synergistic catalytic hydrogenation of furfural to 1, 2-pentanediol and 1, 5-pentanediol with LDO derived from CuMgAl hydrotalcite. *Mol. Catal.* 499, 111298. doi:10.1016/j.mcat.2020.111298
- Fujita, S.-i., Yamanishi, Y., and Arai, M. (2013). Synthesis of glycerol carbonate from glycerol and urea using zinc-containing solid catalysts: A homogeneous reaction. *J. Catal.* 297, 137–141. doi:10.1016/j.jcat.2012.10.001
- Galadima, A., and Muraza, O. (2017). Sustainable production of glycerol carbonate from by-product in biodiesel plant. *Waste Biomass Valorization* 8, 141–152. doi:10.1007/s12649-016-9560-y
- Granados-Reyes, J., Salagre, P., and Cesteros, Y. (2016). *Appl. Clay Sci.* 132–133, 216–222.

and the National Council for Scientific and Technical Research (CONICET).

Conflict of interest

The authors declare that the research was conducted in the absence of any commercial or financial relationships that could be construed as a potential conflict of interest.

Publisher's note

All claims expressed in this article are solely those of the authors and do not necessarily represent those of their affiliated organizations, or those of the publisher, the editors and the reviewers. Any product that may be evaluated in this article, or claim that may be made by its manufacturer, is not guaranteed or endorsed by the publisher.

- Jaiswal, S., Sahani, S., and Chandra Shar, Y. (2022). Enviro-benign synthesis of glycerol carbonate utilizing bio-waste glycerol over Na-Ti based heterogeneous catalyst: Kinetics and E- metrics studies. *J. Environ. Chem. Eng.* 10 (3), 107485. doi:10.1016/j.jece.2022.107485
- Kannan, S., Dubey, A., and Knozinger, H. (2005). Synthesis and characterization of CuMgAl ternary hydrotalcites as catalysts for the hydroxylation of phenol. *J. Catal.* 231, 381–392. doi:10.1016/j.jcat.2005.01.032
- Kim, D.-W., Park, M. S., Selvaraj, M., Park, G. A., Lee, S. D., and Park, D. W. (2011). Catalytic performance of polymer-supported ionic liquids in the synthesis of glycerol carbonate from glycerol and urea. *Res. Chem. Intermed.* 37, 1305–1312. doi:10.1007/s11164-011-0398-4
- Kondawar, S., and Rode, C. (2017). Solvent-free glycerol Transesterification with propylene carbonate to glycerol carbonate over a solid base catalyst. *Energy fuels.* 31 (4), 4361–4371. doi:10.1021/acs.energyfuels.7b00034
- Kuljiraseth, J., Wangriya, A., Malones, J. M. C., Klysubun, W., and Jitkarnka, S. (2019). Synthesis and characterization of AMO LDH-derived mixed oxides with various Mg/Al ratios as acid–basic catalysts for esterification of benzoic acid with 2-ethylhexanol. *Appl. Catal. B Environ.* 243, 415–427. doi:10.1016/j.apcatb.2018.10.073
- Lari, G. M., de Moura, A. B. L., Weimann, L., Mitchell, S., Mondelli, C., and Perez-Ramirez, J. (2017). *J. Mat. Chem. A* 31, 1–13.
- Liu, P., Derchi, M., and Hensen, E. J. M. (2013). Synthesis of glycerol carbonate by transesterification of glycerol with dimethyl carbonate over MgAl mixed oxide catalysts. *Appl. Catal. A General* 467, 124–131. doi:10.1016/j.apcata.2013.07.020
- Luggren, P. J., Apesteguía, C. R., and Di Cosimo, J. I. (2016). Upgrading of biomass-derived 2-hexanol to liquid transportation fuels on Cu–Mg–Al mixed oxides. Effect of Cu content. *Fuel* 177, 28–38. doi:10.1016/j.fuel.2016.02.084
- Lukato, S., Kasozi, G. N., Naziriwo, B., and Tebandeke, E. (2021). Glycerol carbonylation with CO₂ to form glycerol carbonate: A review of recent developments and challenges. *Curr. Res. Green Sustain. Chem.* 4, 100199. doi:10.1016/j.crgsc.2021.100199
- Marimuthu, M., Marimuthu, P., Ashok, A., and Palanivelu, S. (2018). *Mol. Catal.* 460, 53–62.
- Márquez, F., Palomares, A. E., Rey, F., and Corma, A. (2001). Characterisation of the active copper species for the NO_x removal on Cu/Mg/Al mixed oxides derived from hydrotalcites: An *in situ* XPS/XAES study. *J. Mat. Chem.* 11, 1675–1680. doi:10.1039/b009166a
- Pradhan, G., and Sharma, Y. C. (2020). *J. Clean. Prod.* 264, 121258.
- Procopio, D., and Di Gioia, M. L. (2022). An Overview of the latest Advances in the catalytic synthesis of glycerol carbonate. *Catalysts* 12, 50. doi:10.3390/catal12010050
- Rizescu, C., Sun, C., Popescu, I., Urdă, A., Da Costa, P., and Marcu, I. C. (2020). *Catal. Today* 366, 235–244.
- Sahani, S., Upadhyay, S. N., and Sharma, Y. Ch. (2021). Critical review on production of glycerol carbonate from byproduct glycerol through Transesterification. *Ind. Eng. Chem. Res.* 60, 67–88. doi:10.1021/acs.iecr.0c05011
- Sangeetha, A., Jaya Seeli, S., Bhuvana, K. P., Kader, M. A., and Nayak, S. K. (2019). Correlation between calcination temperature and optical parameter of zinc oxide (ZnO) nanoparticles. *J. Sol-Gel Sci. Technol.* 91 (2), 261–272. doi:10.1007/s10971-019-05000-8
- Shen, L., Xia, K., Lang, W., Chu, L., Yan, X., and Guo, Y. (2017). The effects of calcination temperature of support on PtIn/Mg(Al)O catalysts for propane dehydrogenation reaction. *Chem. Eng. J.* 324, 336–346. doi:10.1016/j.cej.2017.05.058
- Shi, J., He, Y., Ma, K., Tang, S., Liu, C., Yue, H., et al. (2021). Cu active sites confined in MgAl layered double hydroxide for hydrogenation of dimethyl oxalate to ethanol. *Catal. Today* 365, 318–326. doi:10.1016/j.cattod.2020.04.022
- Singh, D., Reddy, B., Ganesh, A., and Mahajanind, S. (2014). Zinc/lanthanum mixed-oxide catalyst for the synthesis of glycerol carbonate by Transesterification of glycerol. *Ind. Eng. Chem. Res.* 53 (49), 18786–18795. doi:10.1021/ie5011564
- Sonnati, M., Amigoni, S., Taffin De Givenchy, E., Darmanin, T., Choulet, O., and Guittard, F. (2013). Glycerol carbonate as a versatile building block for tomorrow: Synthesis, reactivity, properties and applications. *Green Chem.* 15 (2), 283–306. doi:10.1039/c2gc36525a
- Valente, J. S., Hernandez-Cortez, J., Cantu, M. S., Ferrat, G., and López-Salinas, E. (2010). *Catal. Today* 150, 340–345.
- Wang, D., Zhang, X., Cong, X., Liu, S., and Zhou, D. (2018). Influence of Zr on the performance of Mg-Al catalysts via hydrotalcite-like precursors for the synthesis of glycerol carbonate from urea and glycerol. *Appl. Catal. A General* 555, 36–46. doi:10.1016/j.apcata.2018.02.009
- Xu, Z. P., and Zeng, H. C. (2000). Decomposition processes of organic-anion-pillared Clays Co₂Mg₅Al(OH)_c(TA)_d·nH₂O. *J. Phys. Chem. B* 104 (44), 10206–10214. doi:10.1021/jp001963n
- Zhang, L., Li, F., Evans, D. G., and Duan, X. (2004). Structure and surface characteristics of Cu-based composite metal oxides derived from layered double hydroxides. *Mat. Chem. Phys.* 87 (2–3), 402–410. doi:10.1016/j.matchemphys.2004.06.010